J. metamorphic Geol., 2001, **19,** 311–325

High-temperature, low-pressure metamorphism and development of prograde symplectites, Marble Hall Fragment, Bushveld Complex (South Africa)

P. PITRA* AND S. A. DE WAAL
Departement Aardwetenskappe, Universiteit van Pretoria, Pretoria 0002, South Africa

ABSTRACT Metapelitic rocks from the Marble Hall Fragment, enclosed in the granites of the magmatic Bushveld Complex, record a two-stage, low-pressure, high-temperature metamorphism. An early paragenesis containing chiastolitic andalusite, cordierite, biotite and quartz ± garnet crystallized in most rocks and equilibrated at 550–600 °C, 0.2 GPa. It was transformed during the second, peak event into various parageneses that commonly coexist within a single thin section. These include garnet–cordierite–biotite–K-feldspar–quartz, sillimanite–cordierite–K-feldspar–quartz and spectacular quartz-undersaturated cordierite–spinel symplectites replacing the chiastolite porphyroblasts.

Based on a detailed phase diagram analysis, we argue that these parageneses result from rapid heating at an approximately constant pressure to temperatures of more than about 720 °C. At these temperatures, the internally buffered activity of water was reduced by incipient water-saturated partial melting, while only minor quantities of melt were produced. Subsequent dry conditions inhibited large-scale equilibration and, together with local inhomogeneities in mineral distribution, led to the development of contrasting parageneses and symplectite textures. No signs of widespread fluid-absent melting of biotite were found, and so the temperature probably did not exceed 760 °C. The peak metamorphic event is attributed to the emplacement of the hot Nebo granite, whereas the early metamorphism was probably caused by the intrusion of one of the phases of the Rustenburg Layered Suite.

We infer the conditions of development of the cordierite–spinel intergrowths and we show that, although symplectites are commonly associated with retrograde processes (cooling and/or decompression), they can record a prograde metamorphic evolution. Furthermore, our contribution emphasizes the importance of the concept of reduced equilibration volume for the understanding and interpretation of some particular textures and parageneses in common rocks.

Key words: Bushveld Complex; contact metamorphism; cordierite–spinel; Marble Hall; symplectite.

INTRODUCTION

Symplectite reaction textures are common in high-grade rocks and their formation is usually ascribed to cooling and/or decompression following the metamorphic peak, i.e. to processes of 'retrograde' character. Cordierite–spinel symplectites replacing sillimanite and/or garnet are reported from many granulite facies terrains. Their formation has generally been attributed to decompression (e.g. Bucher-Nurminen & Droop, 1983; Clarke & Powell, 1991; Waters, 1991; Fitzsimons, 1996; Carson *et al.*, 1997). Cordierite–spinel intergrowths are also known from metamorphic rocks surrounding igneous complexes. They are thought to result from peritectic reactions of sillimanite with melt (Grant & Frost, 1990), or from the local loss of silica following partial melting (Owen, 1991; Srogi *et al.*, 1993; Goodman & Lappin, 1996). Alternatively, Greenfield *et al.* (1998) inferred that such intergrowths formed by the prograde melt-producing breakdown of aluminosilicate + biotite. Finally, similar symplectites are also found replacing andalusite or sillimanite in pelitic xenoliths in magmatic bodies. Zeck (1970), Bouloton (1992), Suárez *et al.* (1992) and Schödlbauer *et al.* (1997), for example, attributed the presence of the cordierite–spinel symplectites to the peraluminous, restitic character of the xenoliths, but a proper petrological analysis and interpretation were not given.

In this paper, we constrain the conditions of formation of the cordierite–spinel intergrowths in high-grade metapelites from the Marble Hall Fragment of the Bushveld Complex. We infer that their formation requires neither widespread partial melting, nor restitic bulk rock compositions, and that symplectites can record a prograde metamorphic evolution.

*Present address: Géosciences Rennes, Université de Rennes I, Campus de Beaulieu — bât. 15, F – 35 042 Rennes Cedex, France (Pavel.Pitra@univ-rennes1.fr).

GEOLOGICAL SETTING

In the region around the town of Marble Hall (Mpumalanga Province, South Africa), volcanic and sedimentary rocks of the Early Proterozoic Transvaal Supergroup form a window — the Marble Hall Fragment — within the Nebo granite of the Lebowa Granite Suite, the youngest member of the Bushveld Igneous Complex (2.05 Ga; Walraven *et al.*, 1990; Walraven & Hattingh, 1993) (Fig. 1). The core of the fragment comprises marble and meta-dolomite of the Chuniespoort Group, overlying a complex of gneiss, schist and amphibolite attributed to the Bloempoort Formation, a possible equivalent of the 2.7 Ga Ventersdorp Supergroup (Hartzer, 1994). The rim of the Marble Hall Fragment consists of metamorphosed shale, quartzite and basic volcanic rocks (Hekpoort andesite and Machadodorp tuff and agglomerate) of the Pretoria Group. The Klapperkop quartzite and the Bevets conglomerate constitute clear marker horizons that allow mapping of the overall structural pattern of the fragment (Fig. 1). Previous work has shown that the volcano-sedimentary rocks of the Marble Hall Fragment have undergone polyphase folding, probably during the emplacement of the basic and ultrabasic Rustenburg Layered Suite of the Bushveld Complex, and form a regional anticline with a NE-plunging axis (de Waal, 1970). Metamorphic grade decreases from the rim towards the core of the fragment and metamorphism is thought to be contemporaneous with folding and related to the emplacement of the Rustenburg Layered Suite (Snyman, 1958; de Waal, 1970). However, detailed information about the metamorphic zoning is lacking, namely due to the very poor outcrop conditions. No petrological information is available about the metamorphism of the marbles and meta-dolomites. Several sills of diorite intrude the Marble Hall Fragment and crop out mostly in the central part. Geochemical and geochronological data suggest that these sills belong to the early intrusion stages of the Rustenburg Layered Suite (de Waal & Armstrong, 2001).

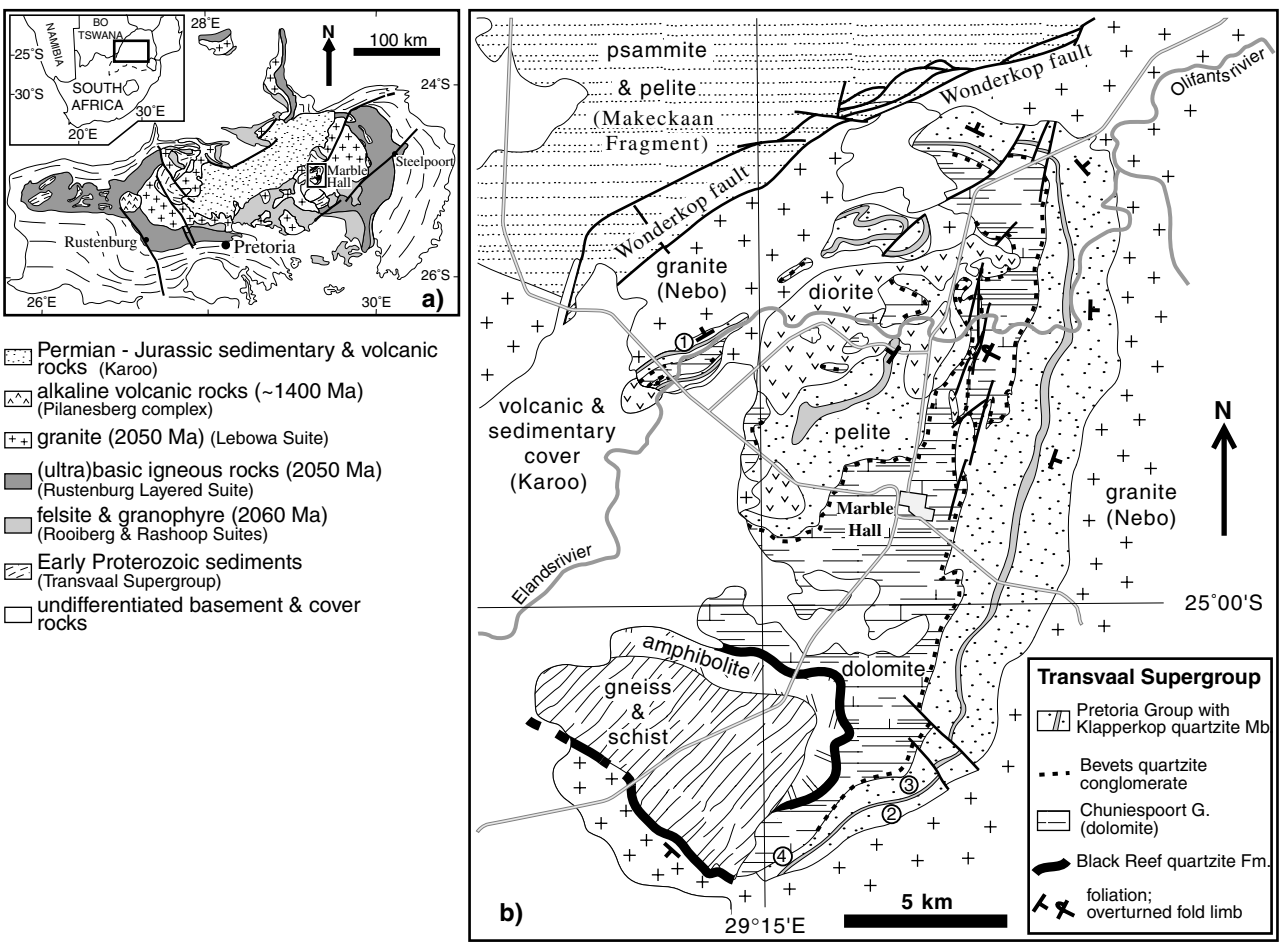

Fig. 1. Map of the Marble Hall Fragment (b), modified after Snyman (1958), de Waal (1970) and Hartzer (1994), and its location within the Bushveld Complex (a). Numbers in circles indicate the location of some of the samples referred to in the text: 1, X527, X532, X566, X567, SAW135; 2, X578, X582; 3, X585; 4, XS.

PETROLOGY

Petrography

The studied rocks are metapelites of the Timeball Hill Formation, collected along the rim of the Marble Hall Fragment, close to the contact with the surrounding granite (Fig. 1). They are dark homogeneous hornfelses and, in places, macroscopic layering can be observed at the hand-specimen scale, corresponding probably to sedimentary bedding. Garnet and chiastolitic andalusite porphyroblasts are frequently present and display a relatively homogeneous distribution in individual hand specimens, although the quantity varies strongly between samples or layers. In the north-western part of the Marble Hall Fragment, very rare centimetre-sized pods of quartzo-feldspathic material are locally present, elongated parallel to the layering.

The matrix of all samples is dominated by cordierite (in general 40–70%), plagioclase, biotite and quartz. Ilmenite is always present, and graphite is generally absent. Matrix cordierite displays a texturally equilibrated mosaic of polygonal grains up to 2 mm in diameter. Small inclusions of quartz, ilmenite and sometimes plagioclase, biotite and exceptionally spinel are concentrated in the cores of cordierite crystals. Matrix plagioclase occurs as equidimensional to slightly elongated, frequently untwinned crystals (generally 0.2–0.5 mm). Biotite forms subhedral flakes up to 1 mm. The mode is highly variable and only rare isolated grains are present in some sections. Quartz crystals are relatively large (up to 1 mm, usually 0.2–0.5 mm), equidimensional and often present a well-equilibrated granoblastic texture. Quartz is common in the matrix, although the mode may be locally as low as 5% (e.g. X567), but is always absent from the parageneses containing spinel. In most samples, K-feldspar is also part of the matrix or forms clusters or large anhedral poikiloblasts (0.5 mm up to 3 mm, locally interstitial) that include the matrix minerals (Fig. 2a). It is often difficult to identify unequivocally in thin sections because it generally shows signs of advanced alteration. Locally, muscovite is present and forms clusters of very fine flakes or exceptionally larger anhedral crystals (up to 0.5 mm) replacing cordierite and feldspar.

This matrix may surround porphyroblasts of garnet and/or chiastolitic andalusite and, in some samples (e.g. X578), primary layering is defined by andalusite-rich layers alternating with layers rich in matrix minerals.

Andalusite forms euhedral to subhedral chiastolite porphyroblasts, 2–20 mm long. Tiny quartz and/or (?)plagioclase inclusions constitute the chiastolite cross, whereas graphite is in general absent. Locally, minute spinel inclusions occur in the outermost part of andalusite crystals.

In many samples, chiastolitic andalusite has been replaced by cordierite–spinel ($\pm$plagioclase) symplectites. Sometimes andalusite is still found in the core (Fig. 2b); in other instances, the transformation is complete, but the trace of the chiastolite cross is often spectacularly preserved (Fig. 2c). Up to 80% of the area of the symplectite is occupied by spinel that occurs as small (around 0.01–0.02 mm) oval green grains. Larger crystals, up to 0.3 mm, are locally found in the cores of the symplectites. A corona of pure cordierite ($\pm$plagioclase) is often present at the rim of the pseudomorph, separating it from the quartz-bearing matrix (Fig. 2b,d). When abundant, biotite is concentrated, together with K-feldspar, around these pseudomorphs (Fig. 2b,d). In altered samples, spinel is transformed to diaspore and cordierite to pinite or fine-grained sericite, but the symplectite textures are still well preserved. In other samples, andalusite recrystallizes topotactically into (generally several) crystals of euhedral prismatic sillimanite (Fig. 2e), up to 2 mm long, the *c*-axis of both minerals being often, but not always, parallel (cf. de Waal, 1970; Vernon, 1987).

Fibrolite is present in some sections and is localized in narrow zones anastomosing around clusters of cordierite and/or andalusite partly replaced by prismatic sillimanite (Fig. 2e).

In the north-western part of the Marble Hall Fragment, garnet in pelitic rocks forms porphyroblasts of variable size ranging from 1 to 10 mm. It can be found in contact with K-feldspar, cordierite and, locally, biotite. Direct contacts with andalusite or spinel were not observed, although cordierite–spinel symplectites are in places present in the vicinity of garnet (e.g. X567) (Fig. 2a,f). Two types of garnet can be distinguished. Anhedral crystals include quartz, ilmenite, biotite and rare cordierite (0.1–0.5 mm). Subhedral to euhedral crystals include ilmenite, cordierite, locally K-feldspar and rare quartz and biotite. Inclusions of cordierite and K-feldspar (ranging in general from 0.2 to 0.5 mm) tend to be concentrated near the garnet rim (Fig. 2f), whereas inclusions of quartz and biotite are tiny and rather occur in the core of the crystals. Small euhedral garnet generally lacks inclusions.

In the southern part of the Marble Hall Fragment, garnet forms subhedral crystals 5–10 mm in diameter (sample XS) and contains abundant inclusions of ilmenite, quartz, plagioclase and biotite. Inclusions are of variable size (up to 1 mm) and show a relatively homogeneous distribution. Contacts with matrix cordierite and biotite are frequent, but K-feldspar is absent in this sample.

Bulk rock and mineral chemistry

Five selected metapelitic samples were analysed by X-ray fluorescence (XRF) and are reported in Table 1. One analysis is taken from Snyman (1958). Compared to average, mostly unmetamorphosed Timeball Hill shales, the samples are relatively poor in silica and alkalis, rich in alumina, and much richer in Fe and Mg (Table 1). However, except for Fe and Mg, they do not

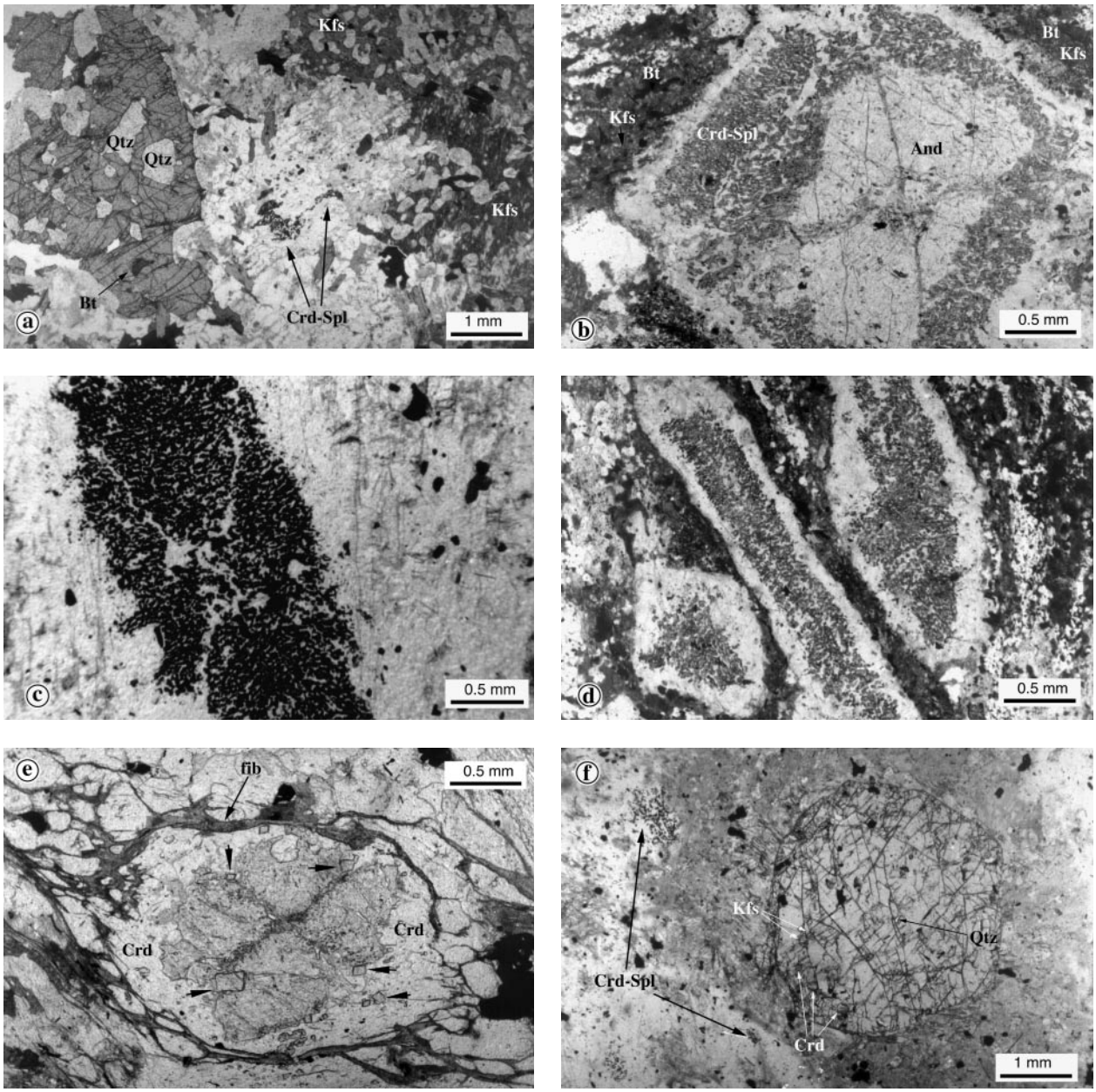

Fig. 2. (a) Anhedral garnet containing inclusions of quartz and biotite (left) and anhedral poikiloblasts of altered K-feldspar (dark grey) containing oval crystals of altered cordierite (light grey, right). A cordierite–spinel symplectite is present close to the garnet, in the middle of the photograph. Sample SAW135. Plane-polarized light. (b) Remnants of chiastolitic andalusite rimmed by a spinel–cordierite symplectite and an altered corona of clear cordierite and (?) plagioclase. Spinel is partly altered to diaspore, cordierite to fine-grained white mica. Sample X578. Plane-polarized light. (c) Cordierite–spinel symplectite replacing andalusite in a matrix of nearly pure cordierite. Although no andalusite is present, the cross-like texture characteristic for chiastolite is still preserved. Sample X527. Plane-polarized light. (d) Altered spinel–cordierite pseudomorphs after andalusite. Note the well-developed spinel-lacking rim of presumably cordierite and plagioclase that separates the symplectites from the quartz-bearing matrix. Biotite and altered K-feldspar are concentrated at the rim of the pseudomorphs. Sample X578. Plane-polarized light. (e) Several crystals of prismatic sillimanite (high relief, diamond shaped, indicated by little black arrows) replacing chiastolitic andalusite. Fibrolite (fib) is concentrated into narrow zones anastomosing around the andalusite–cordierite clusters. Sample X566. Plane-polarized light. (f) Euhedral garnet surrounded by a matrix of altered cordierite, K-feldspar and plagioclase. Inclusions of partly altered cordierite and K-feldspar are concentrated near the rim of the garnet, whereas tiny quartz is preserved in the core. Some cordierite–spinel symplectites are present close to the garnet. Sample X567. Plane-polarized light.

exceed the variations recorded in the unmetamorphosed members of the Timeball Hill Formation (see Reczko, 1994). X_{FeTot} (mol. Fe/(Fe + Mg)) is rather high and ranges from 0.69 to 0.77.

Representative microprobe analyses of individual mineral phases are listed in Table 2. Abbreviations of minerals and mineral end-members are after Kretz (1983). X_{Fe} = Fe/(Fe + Mg); c.p.f.u. = cations per formula unit.

Table 1. Whole-rock XRF analyses of selected samples from the Timeball Hill Formation metapelites in the Marble Hall Fragment.

Oxide	Sample							
(wt%)	X527	X532	X566	X567	X578	XS	av. ETv	sd
SiO_2	46.87	55.87	52.64	47.03	59.57	53.39	54.20	7.85
TiO_2	1.27	0.94	0.81	1.26	0.76	1.00	0.79	0.15
Al_2O_3	26.26	20.94	26.59	26.43	19.02	23.66	24.72	4.78
FeO*	13.23	10.11	9.44	13.19	9.54	10.48	8.08	2.50
MnO	0.09	0.05	0.04	0.09	0.05	0.18	0.02	0.02
MgO	2.94	2.54	1.56	2.94	2.27	4.92	0.72	0.40
CaO	0.89	0.85	0.39	0.75	0.41	1.60	0.11	0.12
Na_2O	0.98	0.47	0.58	0.85	0.51	0.83	0.66	0.60
K_2O	2.64	2.48	2.30	2.34	2.86	1.70	3.48	0.68
P_2O_5	0.08	0.16	0.10	0.07	0.18		0.13	0.09
LOI	2.50	5.10	3.73	2.81	4.28	2.41	4.95	1.55
Sum	97.75	99.51	98.18	97.76	99.45	100.17	99.38	0.75

Garnet. In the north-western part of the Marble Hall Fragment, garnet is chemically homogeneous, rich in almandine ($Alm_{87}Prp_9Grs_3Sps_1$; X_{Fe} = 0.90–0.92), shows no zoning and there is no chemical difference between the two types of garnet. In the southern part of the Marble Hall Fragment, garnet is almandine rich and shows a large homogeneous core ($Alm_{79}Prp_{14}Grs_4Sps_3$; X_{Fe} = 0.85) and a slightly zoned rim ($Alm_{80\rightarrow86}Prp_{13\rightarrow7}Grs_4Sps_3$) with X_{Fe} increasing rimward from 0.86 to 0.92. The proportion of spessartine and grossular is low and stable throughout the grains.

Cordierite. X_{Fe} ranges from 0.51 to 0.69 on a regional scale, but is more homogeneous in individual thin sections. Cordierite is most Fe rich in spinel-bearing samples, where X_{Fe} is in the ranges 0.60–0.64, 0.64–0.69 and 0.62–0.65 in X532, X567 and X578, respectively. There is no significant chemical difference between cordierite in the matrix and in symplectites. However, cordierite included in garnet (sample X567) has a significantly lower X_{Fe} (0.56–0.59). Cordierite is significantly more Mg rich (X_{Fe} = 0.51–0.55) in sample XS,

Table 2. Representative microprobe analyses of principal metamorphic minerals of pelites from the Timeball Hill Formation. Fe_2O_3 in garnet is recalculated on the basis of O = 12, in spinel on the basis of O = 4. m, matrix; CS, cordierite–spinel symplectite; iG, inclusion in garnet.

Sample	X567	X567	XS	XS	X532	X567	X567	XS	X532	X567	X532	X567	X567	XS	XS	X532	X567
Mineral	Grt	Grt	Grt	Grt	Crd	Crd	Crd	Crd	Spl	Spl	Bt	Bt	Bt	Bt	Bt	Plg	Plg
Position	Core	Rim	Core	Rim	CS	iG	m/CS	Matrix	CS	CS	Matrix	Matrix	iG	iG	Matrix	CS	iG
Wt% oxide																	
SiO_2	37.05	36.96	35.87	35.55	47.38	46.37	47.17	47.19	0.00	0.00	33.29	32.27	31.44	32.60	32.51	46.73	57.91
TiO_2	0.00	0.00	0.00	0.00	0.00	0.00	0.00	0.00	0.00	0.17	4.48	3.16	2.68	3.32	5.34	0.00	0.00
Al_2O_3	21.29	21.23	21.12	20.61	33.33	32.49	32.94	33.33	55.86	56.18	19.61	21.12	20.78	20.34	17.82	34.75	26.55
Cr_2O_3	0.00	0.15	0.00	0.00	0.00	0.00	0.00	0.00	0.00	0.37	0.35	0.00	0.60	0.00	0.22	0.00	0.00
NiO					0.00	0.00	0.00		0.00	0.31	0.00	0.00	0.00			0.00	0.00
MgO	2.00	2.05	3.43	1.60	5.13	5.18	4.65	6.61	2.12	1.44	4.80	4.09	3.39	8.38	5.90	0.25	0.00
FeO	37.76	37.57	35.73	38.31	14.10	12.06	15.57	12.14	41.31	39.65	25.64	26.46	26.67	22.27	25.83	0.19	0.14
MnO	0.53	0.40	1.09	1.70	0.00	0.06	0.00	0.14	0.09	0.00	0.00	0.00	0.00	0.00	0.00	0.00	0.00
ZnO					0.00	0.10	0.00		0.52	1.59	0.00	0.00	0.00			0.00	0.07
CaO	1.05	1.07	1.53	1.20	0.00	0.00	0.00	0.00	0.11	0.00	0.00	0.00	0.00	0.00	0.00	16.74	7.40
Na_2O			0.00	0.00	0.22	0.00	0.26	0.31	0.00	0.00	0.24	0.00	0.19	0.38	0.34	1.77	7.12
K_2O			0.00	0.00	0.00	0.00	0.00	0.00	0.00	0.00	9.26	8.91	8.96	8.37	9.10	0.00	0.35
Total	99.68	99.43	98.77	98.97	100.16	96.26	100.59	99.72	100.01	99.71	97.67	96.01	94.71	95.66	97.06	100.43	99.54
No. Ox	12	12	12	12	18	18	18	18	4	4	11	11	11	11	11	8	8
Si	3.01	3.01	2.92	2.93	4.92	4.96	4.91	4.89	0.00	0.00	2.56	2.53	2.51	2.51	2.53	2.14	2.60
Ti	0.00	0.00	0.00	0.00	0.00	0.00	0.00	0.00	0.00	0.00	0.26	0.19	0.16	0.19	0.31	0.00	0.00
Al	2.04	2.04	2.03	2.00	4.08	4.10	4.05	4.07	1.90	1.92	1.78	1.95	1.96	1.84	1.63	1.87	1.41
Cr	0.00	0.01	0.00	0.00	0.00	0.00	0.00	0.00	0.00	0.01	0.02	0.00	0.04	0.00	0.01	0.00	0.00
Fe^{3+}	0.00	0.00	0.14	0.13					0.10	0.06							
Ni					0.00	0.00	0.00		0.00	0.01	0.00	0.00	0.00			0.00	0.00
Mg	0.24	0.25	0.42	0.20	0.79	0.83	0.72	1.02	0.09	0.06	0.55	0.48	0.40	0.96	0.69	0.02	0.00
Fe^{2+}	2.56	2.55	2.29	2.51	1.22	1.08	1.36	1.05	0.89	0.90	1.65	1.73	1.78	1.43	1.68	0.01	0.01
Mn	0.04	0.03	0.08	0.12	0.00	0.01	0.00	0.01	0.00	0.00	0.00	0.00	0.00	0.00	0.00	0.00	0.00
Zn					0.00	0.01	0.00		0.01	0.03	0.00	0.00	0.00			0.00	0.00
Ca	0.09	0.09	0.13	0.11	0.00	0.00	0.00	0.00	0.00	0.00	0.00	0.00	0.00	0.00	0.00	0.82	0.36
Na			0.00	0.00	0.04	0.00	0.05	0.06	0.00	0.00	0.04	0.00	0.03	0.06	0.05	0.16	0.62
K			0.00	0.00	0.00	0.00	0.00	0.00	0.00	0.00	0.91	0.89	0.91	0.82	0.90	0.00	0.02
OH											2.00	2.00	2.00	2.00	2.00		
Total	7.98	7.97	8.00	8.00	11.06	10.99	11.09	11.11	3.00	3.00	9.76	9.76	9.80	9.82	9.81	5.01	5.01
X_{Fe}	0.91	0.91	0.85	0.93	0.61	0.57	0.65	0.51	0.91	0.94	0.75	0.78	0.82	0.60	0.71		
X_{alm}	0.87	0.87	0.79	0.86											X_{an}	0.84	0.36
X_{prp}	0.08	0.08	0.14	0.07											X_{ab}	0.16	0.62
X_{grs}	0.03	0.03	0.05	0.04											X_{or}	0.00	0.02
X_{sps}	0.01	0.01	0.03	0.04													

where it coexists with biotite and garnet, but without spinel and K-feldspar. The Mn content in all samples is below 0.01 c.p.f.u. Na ranges from values below the detection limit to 0.09 c.p.f.u. (recalculated on the basis of 18 O).

Spinel. X_{Fe} ranges from 0.91 to 0.94 (0.91–0.93, 0.93–0.94 and 0.92–0.94 in X532, X567 and X578, respectively). All spinel has low Zn (0.01–0.03 c.p.f.u.), Mn, Ti (both below the detection limit) and Fe^{3+} (0.04–0.14 c.p.f.u., recalculated on the basis of 4 O).

Biotite. In spinel-bearing samples, X_{Fe} ranges from 0.73 to 0.81 (0.73–0.75, 0.75–0.81 & 0.76–0.80 in X532, X567 & X578, respectively) and $X_{Al,M1}$ (calculated as Al + Si-4) comprises between 0.32 and 0.51. There is no clear chemical difference between matrix biotite and that associated with the spinel–cordierite symplectites, but the biotite included in garnet is the most Fe and Al rich ($X_{Fe} = 0.80$–0.82, $X_{Al,M1} = 0.47$–0.52).

In samples lacking spinel and K-feldspar (e.g. XS), matrix biotite is marginally more Mg rich ($X_{Fe} = 0.70$–0.72) and considerably less aluminous ($X_{Al,M1} = 0.16$–0.23) than in spinel-bearing rocks. In these samples, biotite included in garnet is much less Fe rich (X_{Fe} of 0.58–0.65 for $X_{Al,M1}$ of 0.20–0.35) than that in the matrix. The Ti content of biotite in all samples comprises between 0.10 and 0.35 c.p.f.u. (11 O).

K-feldspar. Although no accurate analyses of K-feldspar could be obtained, the rough proportion of elements confirmed in several cases the presence of this mineral. Moreover, least-squares calculations performed with the analysed compositions of minerals and rocks require at least about 5–10% K-feldspar in most rocks.

Plagioclase. This has a variable composition, always relatively rich in anorthite. There is no systematic relation between the plagioclase composition and the geographical position of the samples or the various parageneses. The proportion of anorthite is in the ranges 0.79–0.97, 0.29–0.40, 0.41–0.42 and 0.40–0.58 in samples X532, X567, X578 and XS, respectively.

Paragenetic analysis

Taking into account the mineral chemistry, parageneses can be treated in the classical pelitic system K_2O–FeO–MgO–Al_2O_3–SiO_2–H_2O (KFMASH). Garnet is the only phase containing relatively small, although significant, amounts of Mn. The amounts of Ca present in garnet and those of Ti present in biotite are also relatively small and constant. Although these elements may stabilize garnet and biotite slightly beyond their stability fields in the model system KFMASH, they are not expected to influence the phase relations in a significant way (cf. e.g. Mahar *et al.*, 1997). Plagioclase is then the only phase containing significant amounts of Ca and Na and can therefore be neglected in the analysis of phase relations. Ilmenite, the only phase containing significant proportions of Ti, is treated in the same way.

Table 3. Early and peak mineral parageneses of representative samples (see Fig. 1 for field locations).

Sample	Early paragenesis	Peak paragenesis
X582	Crd–Bt–Qtz ± Kfs	
X566	And–Crd–Qtz–Bt	Sil–Crd–Qtz–Kfs ± Bt
X532, X578	And–Crd–Bt–Qtz	Crd–Bt–Qtz–Kfs
		Crd–Spl ± Bt ± Kfs
X527, X567, SAW135	Grt–And–Crd–Bt–Qtz	Grt–Crd–Bt–Qtz–Kfs
		Crd–Bt–Qtz–Kfs
		Crd–Spl ± Bt ± Kfs ± Grt
XS	Grt–Crd–Bt–Qtz	

The reaction textures show that the rocks experienced at least two major stages of metamorphic crystallization, apart from late alteration. These will be referred to hereafter as 'early' and 'peak' parageneses. However, although the peak parageneses can be observed directly, early parageneses must be deduced from relic minerals, reaction textures and inclusions in large (mostly garnet) porphyroblasts. Some samples (e.g. X582, XS) show no reaction textures, which suggests that the same paragenesis was stable throughout the metamorphic evolution. Mineral parageneses for some representative samples are given in Table 3.

The evolution of phase relations with changing *P–T* conditions and the compatibility of different parageneses in rocks of different bulk composition at the same *P–T* are best understood with the help of compatibility diagrams. Such diagrams are drawn for constant *P–T* and the phases of interest are projected onto a chosen compositional plane from phases with constant chemical potential (phases in excess). However, if projecting phases are of variable composition, the projection plane must lie between the projecting phases and the phases projected, in order to preserve the thermodynamic validity of the final diagram (e.g. Powell & Sandiford, 1988; Worley & Powell, 1998). Unfortunately, it is not possible to draw one convenient compatibility diagram for all of our samples because the only phases common to all parageneses (cordierite and biotite) lie in the middle of the other phases in KFMASH compositional space. On the other hand, at least the most interesting peak stage parageneses can be represented in a diagram projected from biotite, K-feldspar and an aqueous fluid (Fig. 3). We infer from this projection that: (i) the peak parageneses in rocks, or their parts, with different bulk chemistries are mostly compatible under the same *P–T* conditions; and (ii) that spinel and quartz cannot coexist in equilibrium in these rocks. The existence of quartz-bearing peak parageneses and those containing spinel close to one another in the same thin section suggests therefore that equilibration volumes were small and that only local, domainal equilibration was achieved.

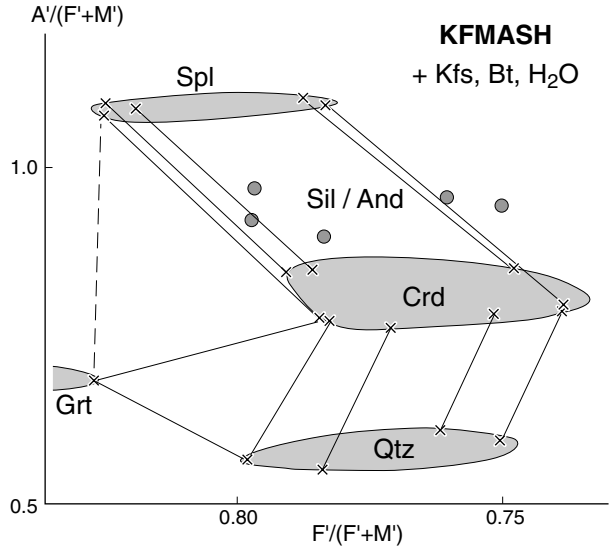

Fig. 3. Compatibility diagram for some of the peak stage parageneses in the system KFMASH. Mineral phases were rigorously projected from the coexisting biotite and end-member K-feldspar and water. The projection plane is the quadrilateral $3FeO.2SiO_2 - 3MgO.2SiO_2$–$FeO.Al_2O_3$–$MgO.Al_2O_3$ in the FeO–MgO–Al_2O_3–SiO_2 tetrahedron, and therefore $A' = Al_2O_3 - 2SiO_2$, $F' = 3FeO.2SiO_2$, $M' = 3MgO.2SiO_2$.

Petrogenetic diagrams and *P-T* estimations

P–T *projection*

As a first step in constraining the *P–T* conditions of the studied samples, a partial petrogenetic grid (*P–T* projection) has been calculated in the chosen model system (KFMASH), starting from the relevant subsystems (KFASH, KMASH), for *P–T* conditions of interest (Fig. 4). The calculations were performed using the software THERMOCALC v. 2.6 (Powell & Holland, 1985, 1988), the internally consistent thermodynamic dataset (September 1997, modified July 1998; Holland & Powell, 1998) and mixing models proposed by Holland & Powell (1998). The grid has been calculated for the minerals observed in our samples — andalusite, sillimanite, garnet, cordierite, spinel, biotite, K-feldspar and quartz. Stable reactions involving staurolite, chlorite and muscovite have also been included because they limit the stability of the parageneses of interest towards low temperatures. Reactions involving orthopyroxene, sapphirine, orthoamphibole, olivine and corundum are not represented for the sake of clarity. These minerals are not present in the studied samples and stable reactions involving them occur either at temperatures mostly higher than those covered by our grid, or do not influence the stability fields of the observed parageneses.

As a consequence of the recent improvements of the thermodynamic dataset used by THERMOCALC and the use of non-ideal mixing models, the topology of our *P–T* grid, around the only KFMASH invariant point (Grt–Crd–Sil–Spl–Bt–Kfs–Qtz–H_2O), differs from that calculated with THERMOCALC and an older version of the thermodynamic dataset by Xu *et al.* (1994). This reflects some important changes in the grid of the subsystem KFASH, because stable KFMASH univariants emanate from stable KFASH invariant points. The most significant difference between the two KFASH projections is that the FASH univariant (degenerate in KFASH) cordierite = hercynite + quartz is not stable in the grid of Xu *et al.* (1994), whereas it is stable at about 0.1 GPa in the *P–T* projection presented here. Thus, all the cordierite-bearing KFASH invariant points at higher pressures become metastable and new ones appear. On the other hand, our grid is in agreement with the empirical qualitative grids of Grant & Frost (1990) and Fitzsimons (1996), although water is considered to be in excess in our grid, whereas melt is the excess phase in the grids of these authors. This point is discussed later.

P–T–X *pseudosections*

Pseudosections (e.g. Hensen, 1971; Guiraud *et al.*, 1990) are the best tool for studying the paragenetic evolution of metamorphic rocks. Calculated for a specific bulk rock composition, these diagrams show directly the mineral parageneses that would crystallize in the studied rock under different *P–T* conditions, rather than the position of the univariant reactional equilibria only. Care is needed, however, in using pseudosections, because the topology and exact position of the various stability fields change with bulk composition. The *effective* bulk composition (Stüwe, 1997) depends on the scale of diffusion efficiency under given conditions and may be difficult to estimate exactly. The major advantage of pseudosections is therefore the identification of the *qualitative P–T* evolution during the rock history. Even so, pseudosections may yield precious quantitative information on *P–T* conditions of metamorphism, if a range of reasonable bulk compositions is examined, or when used together with isopleths of mineral composition.

P–T *pseudosections for analysed bulk compositions*

P–T pseudosections calculated for the analysed bulk rock compositions (Table 1) predict three types of paragenetic sequence at pressures below about 0.3 GPa (Fig. 5a–c). Alumina-poor and Fe-rich rocks (e.g. XS, Fig. 5a) present a single paragenesis — Grt–Crd–Bt–Qtz — between 550 and 800 °C, which is in agreement with the observed absence of reaction textures and lack of K-feldspar in these samples. Biotite becomes progressively more Fe rich and less Al rich with increasing temperature, which is in agreement with compositional differences between biotite included in garnet and that in the matrix.

The And–Crd–Bt–Qtz paragenesis is predicted for Si- and Al-rich, and relatively Fe- and Mg-poor rocks

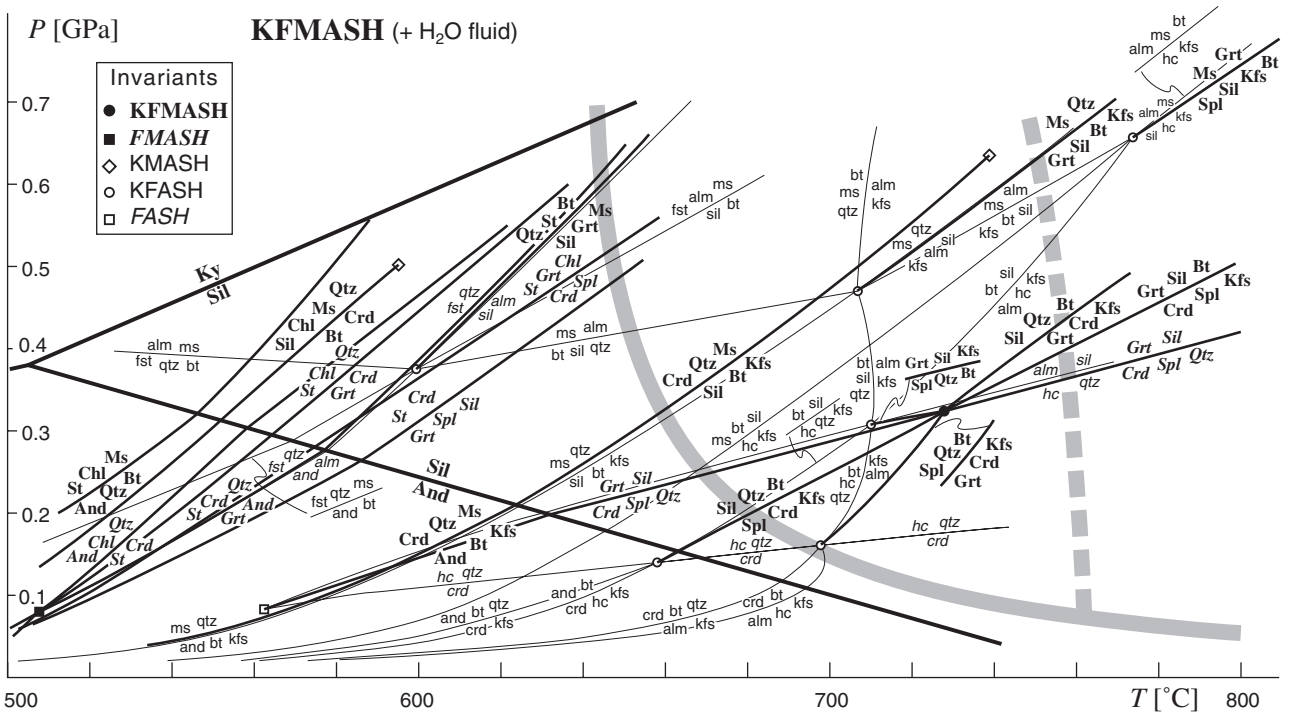

Fig. 4. Partial petrogenetic grid calculated for the minerals and P–T conditions of interest in the system KFMASH and some of the relevant subsystems, using the computer program THERMOCALC. Abbreviations of minerals and mineral end-members are after Kretz (1983). Pure Fe-staurolite is abbreviated as 'fst'. The aluminosilicate system Al_2SiO_5 is indicated by heavy solid lines. Thick lines with bold roman and italic fonts represent univariant reactions in KFMASH and FMASH, respectively. Thin lines with regular roman and italic fonts are reactions in KFASH and FASH, respectively. Filled and open circles and filled and open squares represent KFMASH, KFASH, FMASH and FASH invariant points, respectively. Open diamonds are KMASH invariants. The continuous thick grey line represents the approximate position of the minimum melting curve ($Kfs + Ab + Qtz + H_2O = L$, Keppler, 1989; Ebadi & Johannes, 1991); the broken thick grey line is the position of the fluid-absent biotite melting ($Bt + Plg + Qtz = L + solids$) after Singh & Johannes (1996).

(e.g. X566, Fig. 5b) at lower temperatures (500–620 °C), and is replaced by Sil–Crd–Kfs–Qtz at temperatures above 640 °C. This model fits well the observed replacement of andalusite by sillimanite as well as the fact that biotite is nearly absent in these rocks.

Rocks with slightly less silica and richer in Fe and Mg (e.g. X567, Fig. 5c) display the same And–Crd–Bt–Qtz paragenesis at lower temperatures, but lack sillimanite, forming a Crd–Bt–Kfs–Qtz paragenesis at temperatures of about 600–800 °C. Garnet joins the paragenesis at temperatures above *c*. 760 °C, but does not appear in equilibrium with andalusite at low temperatures in Fig. 5(c). However, locally higher bulk X_{Fe} (e.g. 0.8 instead of 0.7) shifts the low-pressure limit of the Grt–And/Sil–Crd–Bt–Qtz divariant field to low enough pressures that a Grt–And–Crd–Bt–Qtz stability field appears at about 0.15–0.25 GPa, 550–600 °C (Fig. 5c), while the general topology of the pseudosection, at least at the high-temperature side, remains unchanged.

P–T *pseudosections for small equilibration volumes*

The pseudosections calculated for the analysed bulk rock compositions mirror well the main early and peak parageneses. However, they still give insufficient constraints on the P–T conditions of the peak event. Moreover, pseudosections calculated for the spinel-bearing rocks (represented by Fig. 5c) systematically fail to explain the presence of the cordierite–spinel parageneses. This suggests a lack of equilibration on the thin section scale (small equilibration volumes) in rocks presenting either primary local chemical inhomogeneities (e.g. of sedimentary origin) or metamorphic inhomogeneities in the vicinity of the andalusite porphyroblasts. Therefore, pseudosections have been drawn also for bulk compositions based on the modal proportions of minerals, and their chemistry, in parts of spinel-bearing thin sections where equilibrium seems to be attained. Pseudosections calculated for bulk compositions based on matrix parageneses (Crd–Bt–Kfs–Qtz) are topologically identical to those calculated using the bulk compositions analysed (Fig. 5c). The observed proportions and analysed compositions of cordierite, spinel, biotite and K-feldspar in and around the spinel–cordierite symplectites pseudomorphing andalusite yield local bulk compositions relatively poor in silica, and rich in alumina and iron (Fig. 5d). Although the precise composition and therefore the topology of these

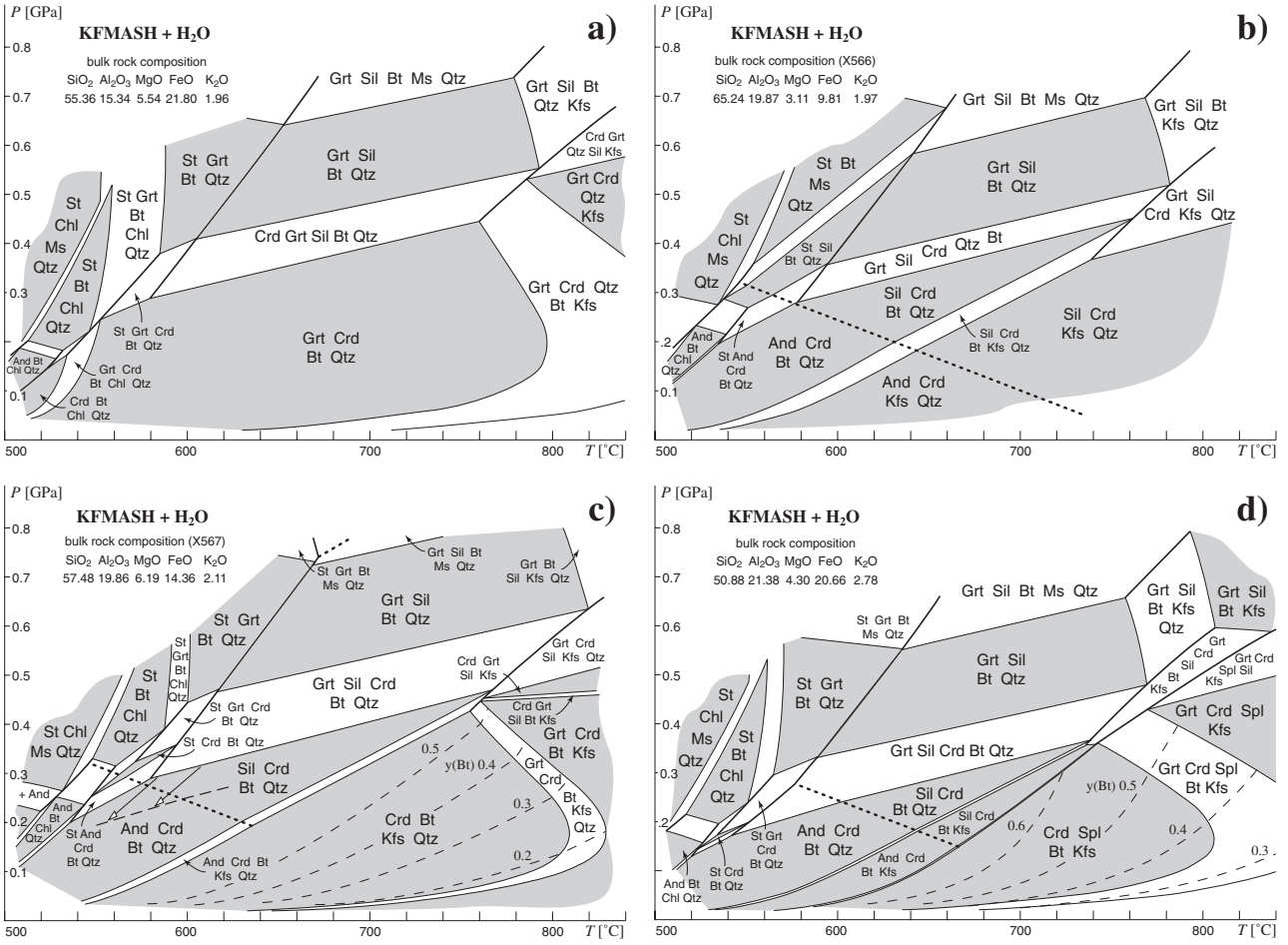

Fig. 5. *P–T* pseudosections calculated with THERMOCALC for the main types of bulk rock compositions of the Timeball Hill pelites in the Marble Hall Fragment: (a) Al-poor, Fe-rich (e.g. XS), (b) Si–Al-rich, Fe–Mg-poor (e.g. X566), (c) intermediate (e.g. X567) compositions. Analysed compositions (Table 1) were corrected for the presence of apatite, ilmenite and plagioclase that cannot be included in the model system KFMASH. An amount of CaO equal to 3.33 that of P_2O_5 was allotted for apatite and subtracted from the bulk rock molar content of CaO. An amount of FeO equal to that of TiO_2 was allotted for ilmenite and subtracted from the bulk rock FeO. An amount of Al_2O_3 equal to that of the remaining $CaO + Na_2O$ and an amount of SiO_2 equal to $2CaO + 6(Na_2O)$ were allotted for plagioclase and subtracted from the bulk rock Al_2O_3 and SiO_2, respectively. Pseudosection (d) was calculated for a local composition corresponding to the area surrounding the pseudomorphed andalusite porphyroblasts using the proportions and compositions of the main constituents (cordierite, spinel, biotite, K-feldspar). Grey fields correspond to stability fields of four-phase, trivariant equilibria; divariant (five-phase) parageneses are white. Thick black lines are parts of univariant reactions from Fig. 4, 'seen' by the particular bulk composition (thick short broken lines are the Al_2SiO_5 polymorph transitions). White-headed arrows in (c) show the displacement of the low-pressure Grt–Sil/And–Crd–Bt–Qtz field boundary with increasing bulk X_{Fe} (0.8 for the long broken line). Light broken lines in (c) and (d) are the isopleths of $X_{Al,M1}$ in biotite, or y(Bt). Some fields are not labelled for the sake of clarity; their parageneses can be deduced from the pseudosection: parageneses in divariant fields contain all the minerals of the neighbouring trivariant fields, trivariant fields contain minerals common to the adjacent divariant fields. Some divariant fields are vanishingly narrow (e.g. St–Grt–Sil–Bt–Qtz in a).

pseudosections depend strongly on the assumed equilibration volume, the resulting pseudosections invariably predict an absence of quartz and the stability of Crd–Spl–Bt–Kfs at high temperatures (at *c.* 660–800 °C, Fig. 5d). Garnet would join this paragenesis at temperatures higher than *c.* 760–800 °C, similar to temperatures of the Grt–Crd–Bt–Kfs–Qtz field in Fig. 5(c).

Isopleths of $X_{Al,M1}$ in biotite (y(Bt) in Fig. 5c,d) were then calculated in order to better constrain the pressure conditions of the peak parageneses. This parameter was chosen rather than X_{Fe}, because it is reasonably pressure sensitive, does not vary significantly with the bulk composition used (or the bulk X_{Fe}) and is less sensitive to late retrograde re-equilibration.

P–T *conditions*

It is difficult to attribute the crystallization of garnet unequivocally to one of the two metamorphic events. The fact that, in some samples (e.g. X567), quartz commonly forms inclusions in subhedral garnet

porphyroblasts, while it is nearly absent from the matrix, suggests that garnet belongs to the early paragenesis Grt–And–Crd–Bt–Qtz. On the other hand, subhedral to euhedral garnet in contact with cordierite and K-feldspar would have crystallized/recrystallized during the peak event (Grt–Crd–Bt–Kfs–Qtz). THERMOCALC calculations show that the composition of garnet is very similar in both early and peak parageneses, and early garnet could therefore be stable during the peak conditions with minor compositional re-equilibration only. Moreover, lower grade garnet often shows prominent growth zoning (e.g. Tracy, 1982), namely in spessartine, and the very homogeneous profile of garnet in K-feldspar + cordierite-bearing samples suggests re-equilibration during the second, peak metamorphic stage. We infer therefore that garnet was stable during both metamorphic episodes.

Interpreting the observed and deduced mineral parageneses and reaction textures with the calculated *P–T* grid (Fig. 4) and pseudosections (Fig. 5a–d) leads to the following constraints on the *P–T* conditions of the two metamorphic events.

1 From the *P–T* projection, the coexistence of garnet + andalusite inferred during the early event requires temperatures of 500–620 °C for pressures below 0.3 GPa (FMASH reactions St + Crd + Qtz = Grt + And and Grt + and = Crd + Spl + Qtz). The pseudosection in Fig. 5(c) further constrains these conditions to about 0.15–0.25 GPa, 550–600 °C. This is corroborated by average *P*, *T* and *P–T* calculations performed with THERMOCALC on the early stage paragenesis (Grt–And–Crd–Bt–Qtz–Plg) of sample X567 (Table 4).

2 Replacement of andalusite by sillimanite suggests heating and/or increase in pressure, whereas the development of spinel–cordierite symplectites on andalusite requires heating and/or decompression due to the positive slope of the various andalusite-consuming, spinel–cordierite-producing reactions (Fig. 4). Both reaction textures, present in samples from the same localities, can therefore be reconciled only in a relatively isobaric *P–T* path involving heating.

3 The stability of garnet with cordierite and K-feldspar during the peak event suggests temperatures as high as 750–800 °C according to pseudosections in Fig. 5(c,d). Moreover, biotite in samples containing spinel appears to have the same composition (y(Bt) = 0.32–0.51) in both types of peak parageneses — (Grt–)Crd–Spl–Bt–Kfs and (Grt–)Crd–Bt–Kfs–Qtz — and information from both pseudosections (Fig. 5c,d) can therefore be combined. Isopleths y(Bt) let us estimate the equilibration conditions of the peak parageneses to be 750–800 °C and 0.1–0.3 GPa for the peak event.

To summarize, the Marble Hall pelites record a two-stage metamorphism, at a relatively stable pressure of about 0.2 GPa, characterized by an increase in temperature from 550–600 °C to more than 750 °C during the peak event.

T–X *pseudosection at 0.2 GPa*

To improve the understanding of the development of the contrasting peak parageneses, and particularly the

Table 4. Summary of the results of average *P*, *T* and *P–T* calculations performed with THERMOCALC on the early paragenesis of sample X567 (Grt–And–Crd–Bt–Plg–Qtz).

Sample		Early stage paragenesis: Grt–And–Crd–Bt–Plg–Qtz										
Phase	X567	Grt			Crd		Bt			Plg	And	Qtz	Fluid
End-member	py	gr	alm	crd	fcrd	phl	ann	east		an	and	q	H_2O
Activity	0.00088	4.00×10^{-5}	0.61	0.22	0.35	0.00338	0.13	0.009		0.58	1	1	1
sd(*a*)/*a*	0.73577	0.83949	0.15082	0.18252	0.12675	2.95858	0.22707	0.49156		0.1	0	0	

Independent set of reactions
(1) py + 5phl + 12and = 4crd + 5east
(2) crd + 2east + q = 2phl + 4and
(3) 4gr + 3phl + 12and = py + 12an + 3east
(4) alm + east + 3q = crd + ann
(5) py + 6gr + 6fcrd + 3east = 4alm + 18an + 3phl

Results — average *P–T*

	T (°C)	sd	*P* (kbar)	sd	correl.
	673	93	3.7	1.0	0.968

Independent set of reactions (excluded end-member: py)
(1) gr + 2phl + 6and = crd + 3an + 2east
(2) 2gr + crd + 2east + 3q = 6an + 2phl
(3) 3gr + crd + ann + 6and = alm + 9an + east
(4) gr + 2crd + 2ann + 6and = 3fcrd + 3an + 2east

Results — average *P*

	T (°C)	450	500	550	600
	av *P*	0.93	1.5	2.1	2.7
	sd	0.19	0.21	0.22	0.23

Independent set of reactions (excluded end-member: py)
(1) 2alm + crd + 2east + 6q = 3fcrd + 2phl
(2) 3alm + 10phl + 5ann + 36and = 12fcrd + 15east
(3) 2alm + 4and + 5q = 3fcrd
(4) 5gr + 3crd + 2ann + 6and = 2alm + 15an + 2phl

Results — average *T*

	P	1.0	1.5	2.0	2.5
	av *T*(°C)	461	500	540	580
	sd	20	20	20	20

Conditions resulting from the simultaneous calculation of *P* and *T* fall in the sillimanite stability field, only the lowermost part of the uncertainty ellipse overlapping with the andalusite field. These results are extremely dependent on pyrope activity, but a set of independent reactions between mineral end-members could not be obtained for this type of calculation when pyrope was excluded. On the other hand, equilibration pressure and temperature could be calculated independently (at given temperature and pressure, respectively), without the information on pyrope activity. Only results falling into the andalusite stability field are reported here. These results yield *P–T* conditions that are basically the same as the region in which the average *P–T* uncertainty ellipse overlaps with the andalusite field.

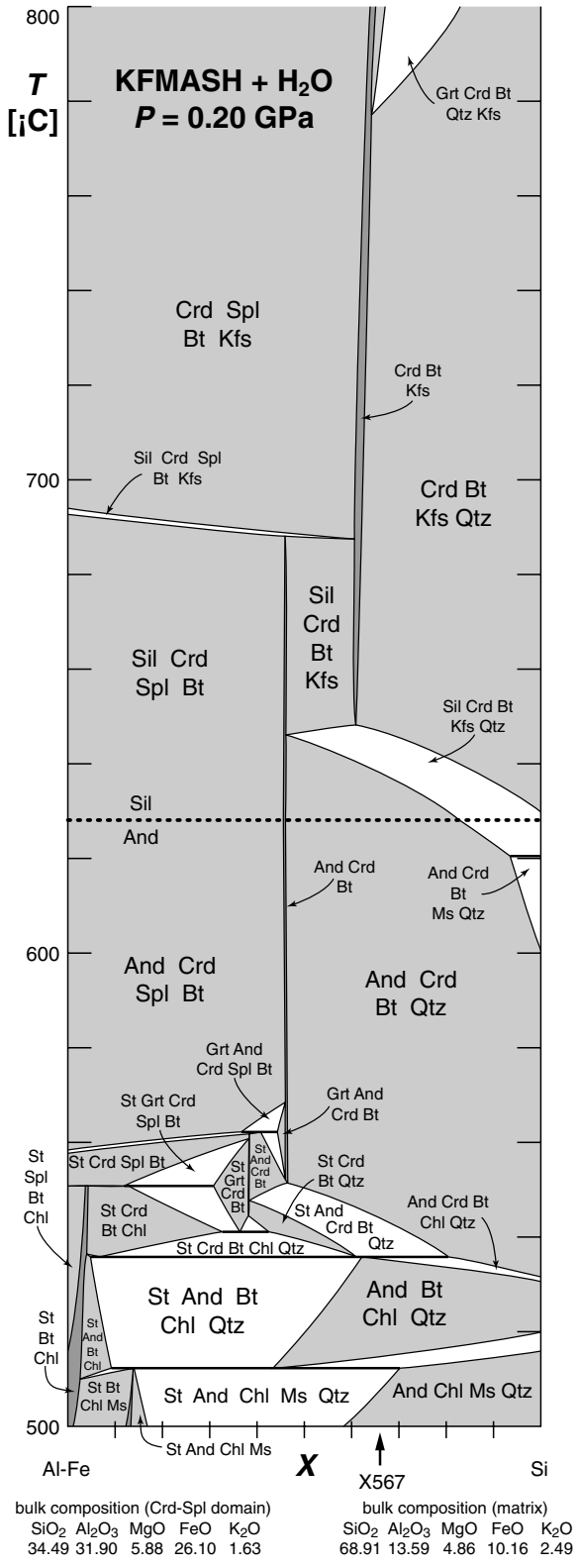

Fig. 6. *T–X* pseudosection for compositions ranging between those of the matrix domains (on the right) and those of the domains around the spinel–cordierite symplectites (on the left). The approximate position of the composition of sample X567 (Fig. 5c) is indicated. The changes along *X* correspond essentially (from right to left) to a decrease in SiO_2, a concomitant increase in Al_2O_3 and FeO, and a slight increase in bulk X_{Fe}. Fields are labelled as in Fig. 5.

spinel–cordierite symplectites, a *T–X* pseudosection was drawn at a fixed pressure of 0.2 GPa (Fig. 6). The compositions represented range between that of the matrix domains and that of the domains around the spinel–cordierite symplectites, which corresponds essentially to a decrease in SiO_2, a concomitant increase in Al_2O_3 and FeO, and a slight increase in bulk X_{Fe}. For extremely Si-poor and Fe–Al-rich compositions (equilibration volumes limited to the Crd–Spl symplectites and the immediate vicinity), quartz is absent and spinel is present even at lower temperatures, yielding undersaturated And–Crd–Spl–Bt$\pm$Grt/St parageneses between 550 and 630 °C. No evidence for the existence of such parageneses during the early metamorphic stage was found.

The lack of these extreme parageneses during early metamorphism means that the development of the contrasting peak parageneses cannot be attributed to primary lithological heterogeneities, but is rather a result of metamorphic processes. We deduce that equilibrium was attained at a relatively large scale during the first event, resulting in the formation of And–Crd–Bt–Qtz$\pm$Grt parageneses, predicted by the pseudosections based on bulk rock analyses (Fig. 5a–c). However, rocks failed to equilibrate, even on a thin section scale, during the second, peak event. This resulted in the formation of quartz-undersaturated spinel–cordierite symplectites replacing andalusite, while quartz-saturated parageneses developed in the matrix.

X–X *pseudosection at 750 °C, 0.2 GPa*

Local inhomogeneities in bulk composition induced by the presence of andalusite crystals after the early metamorphic event cannot alone explain the formation of the cordierite–spinel intergrowths. In fact, in quartz-rich rocks, small equilibration volumes around andalusite porphyroblasts induce a locally Al-rich, but also relatively Si-rich and Fe-poor rock chemistry that would only yield Sil–Crd–Qtz–Kfs parageneses similar to those of Fig. 5(b). Our calculated model phase diagrams show that the development of spinel-bearing parageneses under the *P–T* conditions of interest is governed by the available SiO_2 and is only possible in SiO_2-poor bulk compositions. This is illustrated in Fig. 7, where interactions between an andalusite porphyroblast and a surrounding matrix composed of cordierite and variable proportions of quartz and biotite are represented (cf. Clarke *et al.*, 1995). The

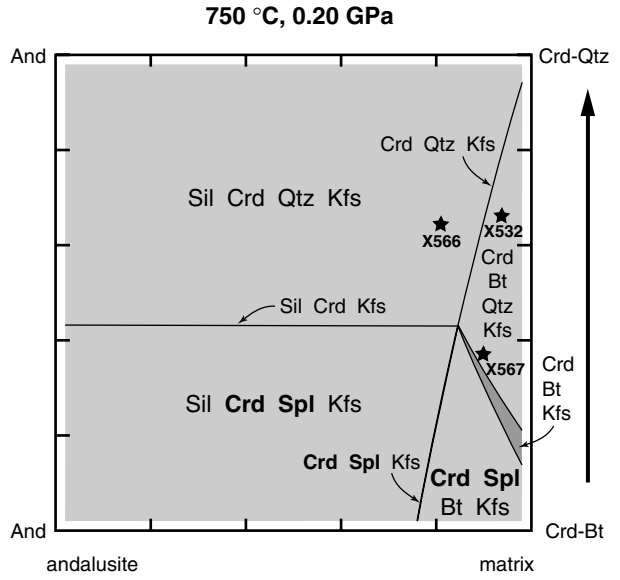

Fig. 7. Compositional pseudosection calculated using THERMOCALC for the model system KFMASH at 750 °C and 0.2 GPa with H_2O in excess. The pseudosection shows the dependence of the peak parageneses on their position between an andalusite porphyroblast and the matrix with different proportions of quartz and biotite. Cordierite is always present in the matrix in large proportions and its quantity does not influence the general appearance of the diagram. Compositions at the corners of the diagram are based on compositions of biotite and cordierite predicted by THERMOCALC for the early And–Crd–Bt–Qtz parageneses. Spinel-bearing parageneses only develop in bulk compositions relatively poor in quartz. Whole-rock compositions of one spinel-free (X566) and two spinel-bearing (X567, X532) samples are also shown.

effective local bulk composition evolves progressively along horizontal lines, corresponding to a specific biotite to quartz ratio, from the andalusite porphyroblast into the matrix, showing the sequence of stable parageneses. Spinel only forms in local compositions relatively poor in quartz. In the light of this diagram, the development of spinel–cordierite symplectites is easy to understand in the initially relatively quartz-poor rocks (e.g. X567). On the other hand, in quartz-rich lithologies (e.g. X532), one has to consider local modal inhomogeneities in the distribution of quartz and biotite, that developed during the early metamorphic event. They would have led to the splitting of the rock composition into parts relatively rich in quartz and parts where andalusite was surrounded by a biotite-rich matrix. The latter yielded the Crd–Spl symplectites during the subsequent peak event.

DISCUSSION

The presented phase diagrams were calculated in a system containing excess water. However, although cordierite and spinel may coexist at temperatures as low as 500 °C (Fig. 4), the development of symplectite textures indicates rapid nucleation but difficult growth of crystals. This generally suggests large overstepping of equilibrium temperatures under conditions of rather ineffective diffusion, most commonly achieved in fluid-deficient environments. High temperatures and dry conditions are corroborated by the common absence of fibrolite and the observed topotactic replacement of andalusite by prismatic sillimanite (cf. e.g. Rosenfeld, 1969; Carlson & Rosenfeld, 1981).

Garnet–cordierite–K-feldspar parageneses with or without spinel are only stable at temperatures as high as *c.* 700 °C under water-present conditions (Fig. 4), and it is clear from Fig. 4 that metamorphism proceeded well above the H_2O-saturated solidus. A low activity of water could produce such parageneses at lower temperatures (cf. Holdaway & Lee, 1977), but low a_{H_2O} is unlikely in upper crustal aluminous metapelites that do not contain graphite, at temperatures below the beginning of partial melting. In fact, water activity in biotite-bearing rocks will be internally buffered to high values by dehydration reactions with increasing temperature until partial melting reactions are encountered (e.g. Powell, 1983a).

Upon heating, the first, water-saturated melting reaction will produce an infinitesimal amount of granitic liquid that strongly fractionates water, lowering the H_2O activity in the system. This shifts the melting reactions to higher temperatures, but decreases the temperatures required to produce new solid phase mineral parageneses (Fig. 8). Thus, water activity is internally buffered to low values and partial melting drives the system to effectively dry conditions, while only minor amounts of melt are produced (e.g. Powell, 1983a,b).

It is beyond the scope of this article to examine the exact topology of *P–T* diagrams in the region beyond the onset of partial melting, and Fig. 8 only tries to approach qualitatively the relations between partial melting and solid phase parageneses. The minimum melting curve in Fig. 4 applies for the water-saturated granite system Kfs–Ab–Qtz (Keppler, 1989; Ebadi & Johannes, 1991) and Fig. 8 shows the behaviour of this solidus as a function of a_{H_2O} (Ebadi & Johannes, 1991). Water-saturated melting in the system KFMASH would begin at higher temperatures, but the addition of plagioclase would shift the melting curves back to lower temperatures (Vielzeuf & Holloway, 1988), which is confirmed by recent THERMOCALC calculations in the system NCKFMASH (R. Powell, 1999 personal communication). The Ebadi & Johannes' fluid-saturated melting curve therefore seems to be a satisfactory approximation of real partial melting reactions for our purpose. Fluid-absent melting of biotite starts at temperatures of about 730–760 °C, at the pressures of interest, according to the various experimental studies (e.g. Le Breton & Thompson, 1988; Singh & Johannes, 1996; Fig. 4).

In the north-western part of the Marble Hall Fragment, the relatively coarse grain size, presence of subhedral grains of cordierite in K-feldspar poikilo-

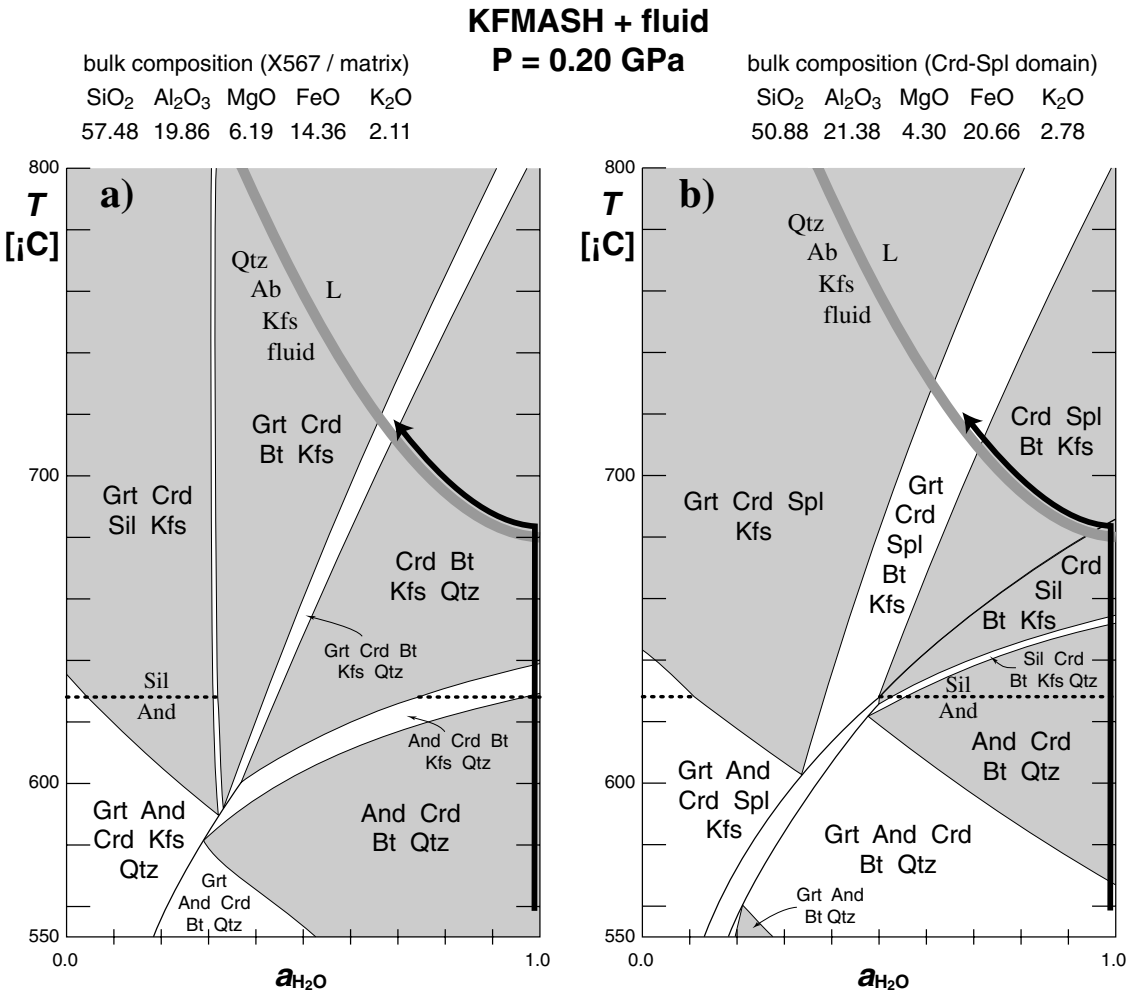

Fig. 8. T–a_{H_2O} pseudosections show the decrease in equilibration temperatures of the peak mineral parageneses with decreasing water activity. (a) is calculated for the bulk composition of sample X567 (Fig. 5c), reflecting the behaviour of matrix domains. The bulk composition used in (b) is that used in Fig. 5(d) and corresponds to an area containing a spinel–cordierite pseudomorph after andalusite. The Kfs–Ab–Qtz solidus (Ebadi & Johannes, 1991) is represented by the thick grey line. The probable evolution of the studied rocks is represented by the thick black arrow. On heating, the system will be first kept at a_{H_2O} values close to unity by biotite dehydration. At the fluid-present solidus, minute quantities of melt will be produced and the system will move along the solidus, the water activity being internally buffered to lower values. Low values of water activity would in turn allow the crystallization of the observed parageneses at lower temperatures.

blasts and the occurrence of rare pockets of quartzofeldspathic material suggest that incipient partial melting may have occurred in these rocks. However, signs of widespread melting were not found, and it is probable therefore that fluid-absent melting reactions, where large quantities of melt are produced (e.g. Powell, 1983b; Clemens, 1990), did not take place. Rapid further heating of the early, andalusite-bearing parageneses to temperatures beyond the onset of partial melting seems to explain the observed textures and mineral parageneses. It appears from Fig. 8 that the parageneses formed at temperatures between 720 and 760 °C, under conditions of reduced water activity.

On the other hand, no signs of partial melting have been observed in the samples from the southern part of the Marble Hall Fragment where cordierite–spinel symplectites are also present. These samples were collected in the immediate vicinity of the contact with the Nebo granite. This intrusion is an A-type granite, crystallized from a presumably very dry, high-temperature magma (Hill *et al.*, 1996). A strong a_{H_2O} gradient should then be expected between the metapelites and the cooling magma. We suggest that this gradient could 'drain' the fluids out of the andalusite-bearing metasediments and would explain the lack of large-scale equilibration and the consequent local development of the cordierite–spinel symplectites.

Symplectites and corona textures are thought to develop due to relatively rapidly proceeding reactions, under conditions of ineffective diffusion and large reaction overstepping, and are generally perceived as features characteristic of retrograde processes (e.g.

Yardley, 1989; Passchier & Trouw, 1996). We show that such textures *can* record a prograde evolution. This conclusion, maybe somewhat counter-intuitive, obviously requires special conditions and cannot be applied to all symplectite occurrences. Greenfield *et al.* (1998) attributed the development of similar cordierite–spinel intergrowths in partially molten, strongly Al-rich pelites to the breakdown of aluminosilicate + biotite in a prograde context. They inferred that the preservation of these textures reflected an interplay of low strain, the reaction sequence and the unusual bulk rock composition. However, the proposed reaction produces magmatic liquid. In this case, one would expect relatively high diffusion rates, incompatible with the development of symplectites. We believe that the deficiency of excess fluids and melts, typical of the *incipient* stages of partial melting, and the subsequent lack of large-scale equilibration, describe better the conditions under which such textures can develop in a prograde environment.

CONCLUSIONS

We have shown that the metamorphic evolution of the pelitic samples from the Marble Hall Fragment presents two main stages.

1 The early stage is characterized by a paragenesis containing chiastolitic andalusite–cordierite–biotite–quartz ± garnet that is common to most rock types and equilibrated at 550–600 °C, 0.2 GPa.

2 During the second, peak event, rocks were rapidly heated at an approximately constant pressure to temperatures of more than about 720 °C, where water-saturated partial melting began. As a result of internally buffered water activity, further heating produced only minor quantities of melt, but reduced the availability and activity of water. Dry conditions, low water activity and local inhomogeneities in mineral distribution inhibited large-scale equilibration and caused the development of contrasting mineral parageneses and particular textures: whereas cordierite–biotite–K-feldspar–quartz ± garnet characterize the matrix, a symplectitic intergrowth of spinel and cordierite has replaced chiastolite porphyroblasts. We argue, on the basis of the calculated phase diagrams, that, unlike most symplectitic textures reported from high-grade terranes, these symplectites have a prograde character. They result from conditions of reduced fluid availability due to either incipient partial melting or, in some instances, to drainage of fluids by abundant adjacent hot and dry magma. We believe that similar processes are responsible for the common formation of cordierite–spinel symplectites replacing andalusite in pelitic xenoliths in granitic magmas.

Both metamorphic stages are of the high-temperature, low-pressure type and are clearly intrusion related. While the second metamorphic event appears to be associated with the emplacement of the Nebo granite, the origin of the first metamorphic stage is less clear. We feel, however, that the drastic increase in temperature recorded during the peak event can be achieved more easily by successive intrusions rather than by progressive heating of the rocks by one large intrusion. The intrusion at the origin of the first metamorphic event must therefore be sought for among the many earlier intrusions that constitute the Bushveld Complex: one of the early intrusions of the basic and ultrabasic Rustenburg Layered Suite may be a good candidate.

ACKNOWLEDGEMENTS

We are thankful to R. Powell, M. Guiraud and M. Ballèvre for stimulating discussions. This article has benefited from constructive reviews by G. Clarke and especially J. Arnold.

REFERENCES

Bouloton, J., 1992. Mise en évidence de cordiérite héritée des terrains traversés dans le pluton granitique des Oulad Ouaslam (Jebilet, Maroc). *Canadian Journal of Earth Sciences*, **29**, 658–668.

Bucher-Nurminen, K. & Droop, G., 1983. The metamorphic evolution of garnet–cordierite–sillimanite–gneisses of the Gruf-Complex, Eastern Pennine Alps. *Contributions to Mineralogy and Petrology*, **84**, 215–227.

Carlson, W. D. & Rosenfeld, J. L., 1981. Optical determination of topotactic aragonite–calcite growth kinetics: metamorphic implications. *Journal of Geology*, **89**, 615–638.

Carson, C. J., Powell, R., Wilson, C. J. L. & Dirks, P. H. G. M., 1997. Partial melting during tectonic exhumation of a granulite terrane: an example from the Larsemann Hills, East Antarctica. *Journal of Metamorphic Geology*, **15**, 105–126.

Clarke, G. L. & Powell, R., 1991. Decompressional coronas and symplectites in granulites of the Musgrave Complex, central Australia. *Journal of Metamorphic Geology*, **9**, 441–450.

Clarke, G. L., Powell, R. & Vernon, R. H., 1995. Reaction relationships during retrograde metamorphism at Olary, South Australia. *Journal of Metamorphic Geology*, **13**, 715–726.

Clemens, J. D., 1990. The granulite–granite connection. In: *Granulites and Crustal Evolution, NATO ASI Series (C)* (eds Vielzeuf, D. & Vidal, P.), pp. 25–36. Kluwer Academic Publishers, Dordrecht.

Ebadi, A. & Johannes, W., 1991. Beginning of melting and composition of first melts in the system Qz–Ab–Or–H_2O–CO_2. *Contributions to Mineralogy and Petrology*, **106**, 286–295.

Fitzsimons, I. C. W., 1996. Metapelitic migmatites from Brattstrand Bluffs, East Antarctica — metamorphism, melting and exhumation of the mid crust. *Journal of Petrology*, **37**, 395–414.

Goodman, S. & Lappin, M. A., 1996. The thermal aureole of the Lochnagar Complex: mineral reactions and implications from thermal modelling. *Scottish Journal of Geology*, **32**, 159–172.

Grant, J. A. & Frost, B. R., 1990. Contact metamorphism and partial melting of pelitic rocks in the aureole of the Laramie anorthosite complex, Morton Pass, Wyoming. *American Journal of Science*, **290**, 425–472.

Greenfield, J. E., Clarke, G. L. & White, R. W., 1998. A sequence of partial melting reactions at Mt Stafford, central Australia. *Journal of Metamorphic Geology*, **16**, 363–378.

Guiraud, M., Holland, T. & Powell, R., 1990. Calculated mineral equilibria in the greenschist–blueschist–eclogite facies in Na_2O–FeO–MgO–Al_2O_3–SiO_2–H_2O: methods, results and

geological applications. *Contributions to Mineralogy and Petrology*, **104**, 85–98.
Hartzer, F. J., 1994. Geology of Transvaal Inliers in the Bushveld Complex. *PhD Thesis*, Rand Afrikaans University, Johannesburg.
Hensen, B. J., 1971. Theoretical phase relations involving garnet and cordierite in the system $MgO–FeO–Al_2O_3–SiO_2$. *Contributions to Mineralogy and Petrology*, **33**, 191–214.
Hill, M., Barker, F., Hunter, D. & Knight, R., 1996. Geochemical characteristics and origin of the Lebowa Granite Suite, Bushveld Complex. *International Geology Review*, **38**, 195–227.
Holdaway, M. J. & Lee, S. M., 1977. Fe–Mg cordierite stability in high-grade pelitic rocks based on experimental, theoretical, and natural observations. *Contributions to Mineralogy and Petrology*, **63**, 175–198.
Holland, T. J. B. & Powell, R., 1998. An internally consistent thermodynamic data set for phases of petrological interest. *Journal of Metamorphic Geology*, **16**, 309–343.
Keppler, H., 1989. The influence of the fluid phase composition on the solidus temperatures in the haplogranite system $NaAlSi_3O_8–KAlSi_3O_8–SiO_2–H_2O–CO_2$. *Contributions to Mineralogy and Petrology*, **102**, 321–327.
Kretz, R., 1983. Symbols for rock forming minerals. *American Mineralogist*, **68**, 277–279.
Le Breton, N. & Thompson, A. B., 1988. Fluid-absent (dehydration) melting of biotite in metapelites in the early stages of crustal anatexis. *Contributions to Mineralogy and Petrology*, **99**, 226–237.
Mahar, E. M., Baker, J. M., Powell, R., Holland, T. J. B. & Howell, N., 1997. The effect of Mn on mineral stability in metapelites. *Journal of Metamorphic Geology*, **15**, 223–238.
Owen, J. V., 1991. Cordierite + spinel parageneses in pelitic gneiss from the contact aureoles of the Mistastin batholith (Quebec) and the Taylor Brook gabbro complex (Newfoundland). *Canadian Journal of Earth Sciences*, **28**, 372–381.
Passchier, C. W. & Trouw, R. A. J., 1996. *Microtectonics*. Springer-Verlag, Berlin.
Powell, R., 1983a. Fluids and melting under upper amphibolite facies conditions. *Journal of the Geological Society, London*, **140**, 629–633.
Powell, R., 1983b. Processes in granulite-facies metamorphism. In: *Migmatites, Melting and Metamorphism. Proceedings of the Geochemical Group of the Mineralogical Society* (eds Atherton, M. P. & Gribble, C. D.), pp. 127–139. Shiva Publishing Ltd, Nantwich.
Powell, R. & Holland, T. J. B., 1985. An internally consistent dataset with uncertainties and correlations: 1. Methods and a worked example. *Journal of Metamorphic Geology*, **3**, 327–342.
Powell, R. & Holland, T. J. B., 1988. An internally consistent dataset with uncertainties and correlations: 3. Applications to geobarometry, worked examples and a computer program. *Journal of Metamorphic Geology*, **6**, 173–204.
Powell, R. & Sandiford, M., 1988. Sapphirine and spinel phase relationships in the system $FeO–MgO–Al_2O_3–SiO_2–TiO_2–O_2$ in the presence of quartz and hypersthene. *Contributions to Mineralogy and Petrology*, **98**, 64–71.
Reczko, B. F. F., 1994. The Geochemistry of the Sedimentary Rocks of the Pretoria Group, Transvaal Sequence. *PhD Thesis*, University of Pretoria, Pretoria.
Rosenfeld, J. L., 1969. Stress effects around quartz inclusions in almandine and the piezothermometry of coexisting aluminium silicates. *American Journal of Science*, **267**, 317–351.
Schödlbauer, S., Hecht, L., Höhndorf, A. & Morteani, G., 1997. Enclaves in the S-type granites of the Kösseine massif (Fichtelgebirge, Germany): implications for the origin of granites. *Geologische Rundschau*, **86**, S125–S140.
Singh, J. & Johannes, W., 1996. Dehydration melting of tonalites. Part I. Beginning of melting. *Contributions to Mineralogy and Petrology*, **125**, 16–25.
Snyman, C. P., 1958. 'n Gneiss, 'n koepelstruktuur en die metamorfose van die Sisteem Transvaal suid van Marble Hall, Transvaal. *Transactions of the Geological Society of South Africa*, **61**, 225–262.
Srogi, L., Wagner, M. E. & Lutz, T. M., 1993. Dehydration partial melting and disequilibrium in the granulite-facies Wilmington complex, Pennsylvania-Delaware Piedmont. *American Journal of Science*, **293**, 405–462.
Stüwe, K., 1997. Effective bulk composition changes due to cooling: a model predicting complexities in retrograde reaction textures. *Contributions to Mineralogy and Petrology*, **129**, 43–52.
Suárez, O., Cuesta, A., Corretge, G. & Fernandez-Suárez, J., 1992. Spinel-bearing inclusions in calc-alkaline granitoids of the Cantabrian and west Asturian Leonese zones, Hercynian Iberian belt. *Bulletin de la Société Géologique de France*, **163**, 611–623.
Tracy, R. J., 1982. Compositional zoning and inclusions in metamorphic minerals. In: *Characterization of Metamorphism Through Mineral Equilibria* (ed. Ferry, J. M.). *Reviews in Mineralogy*, **10**, 355–397.
Vernon, R. H., 1987. Oriented growth of sillimanite in andalusite, Placitas–Juan Tabo area, New Mexico, U.S.A. *Canadian Journal of Earth Sciences*, **24**, 580–590.
Vielzeuf, D. & Holloway, J. R., 1988. Experimental determination of the fluid absent melting relations in the pelitic system. *Contributions to Mineralogy and Petrology*, **98**, 257–276.
de Waal, S. A., 1970. Interference folding of Bushveld-Igneous-Complex age in the Transvaal system north of Marble Hall, Transvaal. In: *Symposium on the Bushveld Igneous Complex and Other Layered Intrusions. The Geological Society of South Africa Special Publications* (eds Visser, D. J. L. & von Gruenewaldt, G.), pp. 283–298. Geological Society of South Africa, Johannesburg.
de Waal, S. A. & Armstrong, R. J., 2001. The age of the Marble Hall diorite, its relationship to the Uitkomst Complex, and evidence for a new magma type associated with the Bushveld Complex. *South African Journal of Geology*, **103**, 128–140.
Walraven, F., Armstrong, R. A. & Kruger, F. J., 1990. A chronostratigraphic framework for the north-central Kaapvaal craton, the Bushveld Complex and the Vredefort structure. *Tectonophysics*, **171**, 23–48.
Walraven, F. & Hattingh, E., 1993. Geochronology of the Nebo Granite, Bushveld Complex. *South African Journal of Geology*, **96**, 31–41.
Waters, D. J., 1991. Hercynite–quartz granulites: phase relations and implications for crustal processes. *European Journal of Mineralogy*, **3**, 367–386.
Worley, B. & Powell, R., 1998. Singularities in NCKFMASH ($Na_2O–CaO–K_2O–FeO–MgO–Al_2O_3–SiO_2–H_2O$). *Journal of Metamorphic Geology*, **16**, 169–188.
Xu, G., Will, T. M. & Powell, R., 1994. A calculated petrogenetic grid for the system KFMASH, with particular reference to contact-metamorphosed pelites. *Journal of Metamorphic Geology*, **12**, 99–119.
Yardley, B. W. D., 1989. *An Introduction to Metamorphic Petrology*. Longman Scientific & Technical, New York.
Zeck, H. P., 1970. An erupted migmatite from Cerro del Hoyazo, SE Spain. *Contributions to Mineralogy and Petrology*, **26**, 255–246.

Received 15 May 2000; revision accepted 27 November 2000